CSCE Annual Conference

Growing with youth – Croître avec les jeunes

Laval (Greater Montreal)

June 12 - 15, 2019

COMPRESSION LAP SPLICE OF GFRP BARS IN CONCRETE COLUMNS

Amirhomayoon Tabatabaei,[1] Abolfazl Eslami,[1] Hamdy M. Mohamed,[1] and Brahim Benmokrane[1]

[1] Department of Civil Engineering, Université de Sherbrooke, Sherbrooke, Quebec, Canada.

Abstract: Recent years have seen valuable research work on using glass-fiber-reinforced-polymer (GFRP) bars in reinforced-concrete (RC) members under compression. Nonetheless, lap splicing of GFRP bars under compression has not yet been explored with due consideration of its components. To address this knowledge gap, this paper comparatively demonstrates the results of an experimental investigation pertaining to the effect of splice length on the compression lap splicing of GFRP bars in concrete columns. The experiment comprised 5 large-scale circular columns measuring 300 mm in diameter and 1600 mm in height. All columns were tested under a monotonically increasing concentric load. The test variables included the splice length of GFRP reinforcement. The results were compared in terms of the stress–strain curves, ultimate loading, displacement capacity, and splice strength. As the strength of a compression splice consists of end-bearing and bond components, the contribution of each part was scrutinized in detail using measured strain values. The required splice length for GFRP bars was considerably based on the end-bearing component. Based on the experimental results, a length of $8d_b$ can reliably be considered as the required splice length for No. 5 GFRP bars in compression.

1. INTRODUCTION

Corrosion of steel reinforcing bars stands out as a significant factor limiting the life expectancy of reinforced-concrete infrastructure exposed to harsh environmental conditions. In the last decade, the use of fiber-reinforced polymer (FRP) as an alternative reinforcing material in reinforced-concrete (RC) structures has emerged as an innovative solution to the corrosion problem (ACI 440.1R-15). Extensive research programs have been conducted to investigate the flexural and shear behavior of concrete members reinforced with FRP bars (Zadeh and Nanni 2017; Razaqpur and Spadea 2015; Tottori and Wakui 1993; Guadagnini 2006; Ali et al. 2016; Bentz et al. 2010; El-Gamal et al. 2005; El-Sayed et al. 2012; Farghaly and Benmokrane 2103; Hassan et al. 2014). FRP design provisions for shear and flexure are now well established and included in codes and design standards.

Nevertheless, current guidelines do not cover the subject of FRP-reinforced concrete members subjected to axial compression loads. Using GFRP bars as the main reinforcement in compression members is still under consideration. This can be partly attributed to the insufficient recognition of certain parameters that influence the analysis and design of such members. Recently, valuable research work has been conducted to investigate the effect of different parameters on the behavior of concrete members reinforced with GFRP bars subjected to compression axial loads or simultaneous flexural loads (Luca at al. 2010; Tobbi et al. 2014; Afifi et al. 2014; Afifi et al. 2014; Hadi et al. 2016; Hadhood et al. 2017; Hadhood et al. 2017; Hadhood

et al. 2017). The outcomes of these experimental studies may ultimately provide a convincing case to allow the limited use of FRP bars in columns.

While numerous research endeavors have elaborated on the use of FRP bars as the main reinforcement in compression elements, lap splicing of FRP bars in compression has not been explored in detail. It should be noted that, due to considerations such as ease of storage and transportation, FRP bars are manufactured in certain lengths. Thus, splicing is inevitable in reinforced-concrete structures, although it should be minimized in field applications. In such cases, the resistance of a bar spliced along its length is mainly governed by the splice strength. Inadequate splicing can lead to undesirable failure of the member. The pioneering scrutiny of compression splicing dates back to over 40 years ago in which Pfister and Mattock (Pfister and Mattock 1963) examined the requisite length for spliced steel bars in compression. Based on their experimental findings, the strength of a spliced steel bar comprises two components-end bearing and bond-as depicted in Figure 1. The main motivation behind the current experimental campaign aimed at describing the performance of compression lap-spliced GFRP bars in concrete columns with different splice lengths.

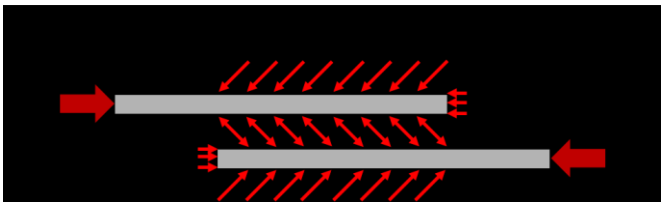

Figure 1. Components of compression lap spliced bars.

2. EXPERIMENTAL PROGRAMME

2.1. Material Properties

All of the specimens were cast on the same day with normal-weight, ready-mix concrete. The 28-day compressive strength of the concrete, determined by the average test results of five cylinder samples (100×200 mm), was about 40.5 MPa. On the testing date, the compressive strength of the concrete cylinders was around 49.3 MPa.

The GFRP-reinforced columns had No. 5 (15.9 mm diameter) sand-coated bars as longitudinal reinforcement and No. 3 (9.5 mm diameter) sand-coated spirals as transverse reinforcement. Figure 2 provides an illustration of the GFRP reinforcement. The tensile properties of the GFRP bars were determined according to the ASTM D7205-06 test method. The mechanical properties of the GFRP bars are provided in Table 1, respectively.

Table 1. Mechanical properties of GFRP reinforcment.

Bar number	Diameter (mm)	Area (mm^2)	Modulus of elasticity (GPa)	Garanteed tensile strength (MPa)	Tensile strain (%)
#3	9.5	71	54.1	1206[1]	2.2
#5	15.9	198	51.2	1374	2.7

[1] Based on the results of straight bars.

Figure 2. Sand-coated GFRP spirals and straight reinforcement.

2.2. Test Specimens

The experimental program aimed at investigating the effects of splice length on the strength of lap-spliced bars under compression. To pursue this objective, 5 circular concrete columns were constructed and tested under monotonically increasing load. The columns specimens were reinforced with GFRP bars. One column was reinforced with continuous bars and used as reference specimens, while all the other specimens were reinforced with spliced bars. All of the specimens measured 300 mm in diameter and 1600 mm in height. All of the columns had a clear concrete cover of 25 mm to the spiral reinforcement as well as a concrete cover of 20 mm on both column bottom surfaces. The geometric and reinforcement details of the test specimens are illustrated in Figure 4.

In this study, the spiral pitch at the central half of the columns was taken as 80 mm (center-to-center) using No. 3 GFRP spirals for the GFRP-reinforced concrete columns. The pitch was reduced to 40 mm at both ends to ensure failure in the spliced region. Plastic ties were used to fasten the spliced bars together and the spirals to the longitudinal reinforcement. In addition, the position of splices with zero lap length was secured with wooden sticks.

All of the cages were made with special attention to the tolerance of approximately ±2 mm. The columns were cast vertically in cylindrical molds made of composite materials. Before casting, all of the molds were adjusted to ensure the verticality of the columns. Figure 4 shows the column fabrication process. The day after casting, all of the columns were unmolded and cured with wet burlap for seven days before storing them in the laboratory at ambient temperature. Table 2 provides the details of the test specimens.

Table 2. Details of test specimens.

Specimen designation	Longitudinal Reinforcement	Splice length, l_s (mm)		Spiral pitch
G5-L0-80	6 #5	0	0	80
G5-L4-80	6 #5	4db	64	80
G5-L8-80	6 #5	8db	128	80
G5-L24-80	6 #5	24db	384	80
G-5-LC-80	6 #5	CONTINUOUS		80

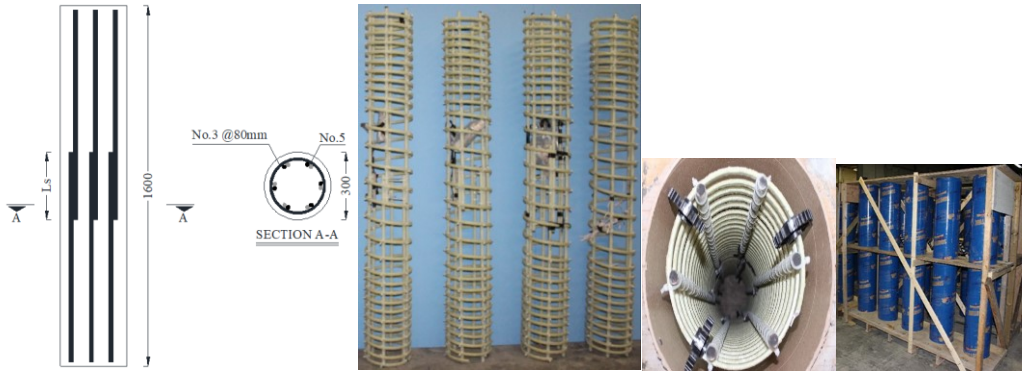

a) b) c) d)

Figure 4. a) Geometric and reinforcement details of the test specimens, (b) assembled cages, (c) GFRP cages inside the formwork, and (d) wooden formwork and Sonotubes.

2.3. Instrumentation and Test Setup

The experiment was carried out under a monotonically increasing concentric load with a rate of 0.5 kN/s. The testing was continued until the load dropped to a level of approximately 65% of the ultimate strength. Figure 5 shows the testing machine and a typical column under loading.

To help ensure the uniform distribution of load, both ends of the specimens were leveled with a thin layer of high-strength cementitious grout prior to testing. These parallel layers can also mitigate load eccentricity. Although the end portions of the specimens were reinforced with more dense spirals, they were additionally confined by steel collars during loading to prevent premature failure at the end regions.

During loading, the strain variations in the longitudinal bars were measured with a set of electrical strain gauges. Figure 5 shows the position of these strain gauges. The contribution of end bearing and bond was distinguished by attaching gauges at the beginning and end of the splice region of a longitudinal bar. To allow for strain development in the bars, the gauges were mounted at a distance of 20 mm from the end of each spliced bar. For the columns with zero splice length, only two strain gauges were installed at the end of the spliced bars. Moreover, in the columns with continuous bars and control specimens, three strain gauges were mounted at the mid-length of three bars, 120° apart along the section perimeter to ensure load eccentricity.

Column axial deformation was measured with four linear variable differential transformers (LVDTs) installed on the four sides of the columns as depicted in Figure 5.

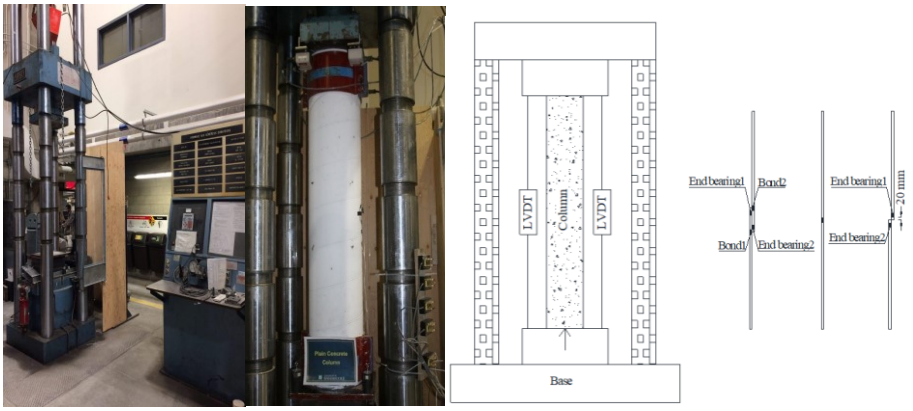

Figure 5. Testing machine position of strain gages and LVDTs.

3. Experimental Results and Observations

The experimental data obtained during loading consisted of strains reinforcement bars, loading capacity, and longitudinal displacement. Table 3 provides a comparison of the mean stress values for all of the columns at the ultimate point. These stresses were determined based on the stress–strain behavior of the

reinforcement. The concrete strain values were recorded up to the spalling of the concrete cover. Table 3 presents the mean values of maximum strains measured by the strain gauges in each column.

Table 3. Summary of results for all test specimens.

Specimen Designation	P (kN)	Failure mode*	f_{sc} (MPa)	f_e (MPa)	f_b (MPa)	Dis. at slippage (mm)
G5-L0-80	2871	S	62	62	-	4.0
G5-L4-80	3213	CS	126	79	47	5.3
G5-L8-80	3255	CS	134	82	52	4.6
G5-L24-80	3276	CS	140	78	62	5
G5-LC-80	3290	B,C	145	-	-	5.2

*C is concrete crushing; S is bar slippage and cover spalling at an upper load; B is bar buckling; CS is cover spalling and bar slippage simultaneously and R is rupture of spirals.
Note: f_{sc} is the splice strength; f_e is the stress developed by end bearing; f_b is the stress developed by bond; and NA is not available.

3.1. Modes of Failure

The failure of the specimens with spliced bars occurred primarily due to concrete-cover spalling and bar sliding. In specimens with short splices, the spliced bars slid with cracks appearing on the column surface; loading continued up to concrete-cover spalling. This behavior was observed in the specimens reinforced with zero-spliced GFRP bars (G5-L0-80). The specimens with longer splice lengths, however, sustained higher loads. The load–displacement curves for these specimens exhibited ascending branch nonlinear behavior at 70% to 80% of peak load (Figure 7) with the appearance of hairline cracks. The load-carrying capacity increased up to cover spalling. Bar sliding and cover splitting took place simultaneously in G5-L4-80, G5-L8-80, and G5-L24-80 at peak load. Figure 8 and Figure 9 show the typical failure modes and overview of the collapsed specimens, respectively. Deep longitudinal cracks, as shown in Figure 9, imply buckling of the longitudinal reinforcement as a failure mode for the specimens constructed with continuous bars. The plateau area in the descending branch for these specimens can be seen in Figure 7. Due to the lack of confinement, the second peak load was not distinctive. Crushing of the concrete core and bar buckling occurred in G5-LC-80.

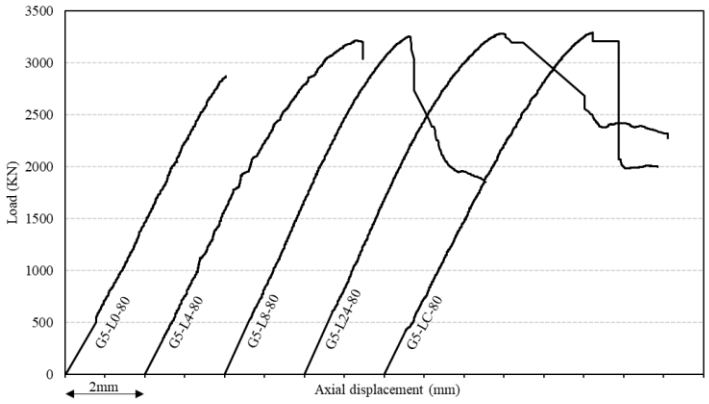

Figure 7. Load vs. axial deformation curves for the test specimens.

3.3. Sliding of Reinforcement

For the specimens with splices, a decrease in the strain value of a spliced bar with increasing total load was assumed to indicate bar slippage (Chun et al. 2010). The load corresponding to this threshold was considered as the ultimate load. This behavior was clearly observed in G5-L0-80. The sliding of GFRP bars with longer splice lengths occurred at peak load. A sharp drop in strain in longitudinal bars was observed after concrete-cover spalling. The concrete remaining around the bars couldn't keep them in place and

transfer the stress between them. The descending branch of the load–displacement curves (Figure 7) also showed sharp drops without significant post-peak responses. Thus, the spliced GFRP bars slid after cover splitting. The corresponding load was considered as the ultimate load capacity of the spliced bars.

3.4. Components of Splice Strength

The strength developed by each component was distinguished with strain gauges at the beginning and end of the spliced bars. To illustrate, Figure 10 shows the load distribution versus measured strain in G5-L8-80 and G5-L24-80 in terms of end-bearing and bond contributions separately. End bearing typically increased linearly up to the ultimate load, as shown in Figure 10. At low levels of loading, the end-bearing portion was much higher than the strain developed by bond. Therefore, the end-bearing contribution was more pronounced in the loading capacity of columns at lower load levels. The contribution of bond strain, however, became more significant as the applied load increased. As shown in Figure 10, the bond contribution at an initial level of loading was insignificant, as indicated for G5-L8-80 and G5-L24-80. It increased rapidly, however, approaching the ultimate load. Figure 10 also provides the strain distribution of the continuous bars in G5-LC-80. As observed, the strain increased nonlinearly up to bar buckling.

The maximum strain measured by strain gauges before bar slippage was multiplied by the reinforcement elastic modulus and considered as end-bearing and bond strength, as presented in Table 3. End-bearing strength ranged from 53 to 82 MPa, irrespective of splice length. The bond strength, however, increased from 46 to 72 MPa proportionally to the increase in splice length.

a) b) c) d)

Figure 8. Typical failure mode: (a) concrete-cover spalling, (b) concrete crushing, (c) rupture of GFRP stirrups, and (d) GFRP-bar buckling.

G5-L0-80 G5-L4-80 G5-L8-80 G5-L24-80 G5-LC80

Figure 9. Overview of the column specimens after failure.

3.5. Splice Length and Strength

In general, increasing the splice length induced a rise in the load-carrying capacity of the columns. Table 3 provides the splice strength and its components for each specimen. A comparison of G5-L8-80 and G5-L4-80 indicates that splice strength would not be linearly proportional to the splice length.

Due to the zero splice length in G5-L0-80, its reinforcement strength was limited to the end-bearing component (equal to 62 MPa). Increasing the splice length from zero (G5-L0-80) to 64 mm (G5-L4-80) yielded a splice strength of 126 MPa. The increased splice length in G5-L8-80 and G5-L24-80 improved the splice strength to 134 MPa and 140 MPa, respectively.

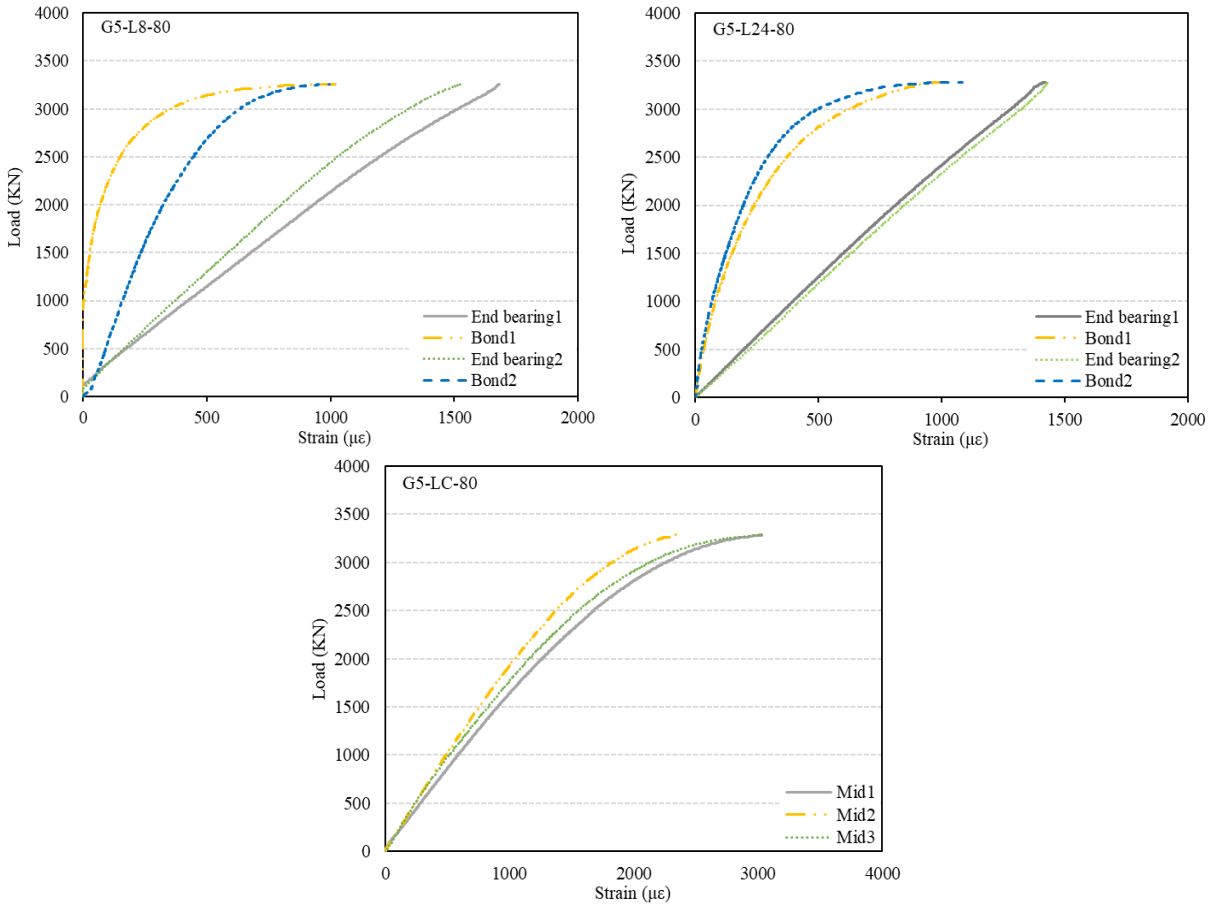

Figure 10. Load vs. end bearing, bond, and mid-strain for G5-L8-80, G5-L24-80, and G5-LC-80 (1, 2, and 3 denote the location of strain gauges).

4. Discussion

4.1. End-Bearing Contribution

The stress values developed by end bearing in the specimens were normalized by the square root of concrete compressive strength and presented in Figure 11. The end-bearing contribution is irrelevant to splicing length and remained nearly constant for all of the specimens. The average value and the coefficient of variation of the normalized end bearing for all the GFRP-reinforced specimens were calculated, respectively, as 10.2 and 0.17 (Figure 11). In other words, the mean strength developed by end-bearing performance was determined to be $10.2\sqrt{f_c'}$, which would be equal to 72 MPa, given the compressive strength of concrete of 49.3 MPa.

4.2. Bond Contribution

Compression force adversely influences the bond contribution due to the lower tensile capacity of concrete under a combined tension and compression stress state (Beskos 1974; Kupfer and Gerstle 1969; Richart et al. 1928). As both compression and tension splices produce circumferential tensile stresses, the tensile capacity of concrete can considerably influence bond strength. Thus, the bond strength in a compression splice is lower than in a tension splice.

The bond stress was calculated by deducting the end-bearing strain from the total strain developed in the spliced bars (see Figure 12). According to the regression analysis of the experimental data, the bond strength of a spliced GFRP bar under compression can be expressed by

$$f_{bond} = \left(2.63\sqrt[4.8]{l_s}\right)\sqrt{f_c'} \quad (1)$$

The coefficient of determination (R^2) for Eq. (1) was determined to be 0.83, implying good correlation between the predicted and experimental results. As shown in Figure 12, the bond strength would generally improve by increasing the splice length. This increment is more evident at shorter splice lengths. The stress developed in G5-L24-80 reached approximately the same load level as the specimen with continuous GFRP bars (difference of less than 8%). In addition, the stress value in the spliced GFRP bar in the specimen with $8d_b$ was about 134 MPa, which is 92% of the target stress developed in the GFRP bar in G5-LC-80. Thus, for the conditions considered in construction of the column specimens in this study, a length of $8d_b$ can be reliably considered as the required splice length for No. 5 GFRP bars in compression. Regarding Figure 12, the values predicted by Eq. (1) for short splice lengths is in good agreement with the experimental results.

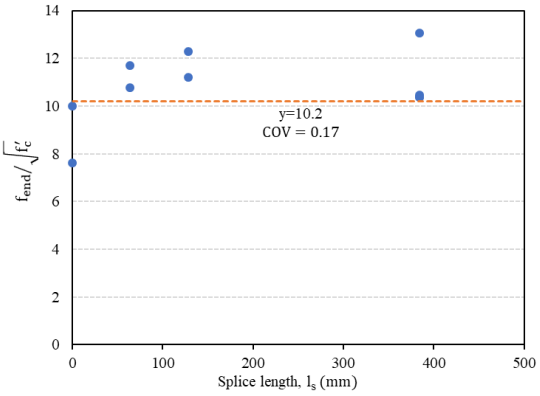

Figure 11. End-bearing contribution to the splice strength in the GFRP specimens.

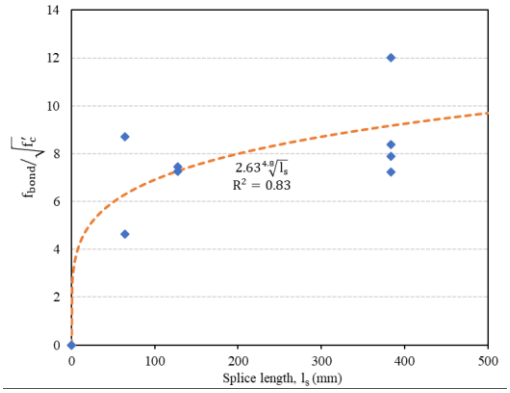

Figure 12. Bond contribution to the splice strength of the GFRP bars.

5. Conclusions

This study is part of an ongoing research program at the University of Sherbrooke investigating the structural performance of GFRP-reinforced concrete columns under axial loads. A total of 5 large-scale RC

columns were prepared and tested to scrutinize the required lap-splice length for GFRP bars under compression. The influence of compression splice length on the strength of the spliced bars was assessed. The following concluding remarks are based on the analysis of the experimental results.

1. Specimens constructed with spliced GFRP bars failed by cover spalling, followed by bar sliding at the splice region. Buckling of GFRP bars occurred in the specimens reinforced with continuous bars. Buckling of spliced bars led to GFRP spiral rupture.

2. The spliced GFRP bars failed to sustain the axial load at a load level corresponding to the appearance of the surface cracking in the specimens with shorter splices or simultaneously with cover spalling in the specimens with longer splices.

3. The test observations revealed that the splice strength of the GFRP bars would not be linearly proportional to the splice length. The bond strength is proportional to a power of splice length.

4. As the strength of the compression splice consists of end-bearing and bond components, the contribution of each part was scrutinized in detail in this study using measured strains. The test results indicate that the end-bearing strength of the spliced GFRP bars increased linearly up to peak load and contributed significantly to the splice strength, much more so than does the bond strength. Upon crack initiation, the bond-strength component became more active in contributing to the splice strength.

5. Finally, it was found that a length of $8d_b$ can be reliably considered as the required splice length for No. 5 GFRP bars in compression. Based on the regression analysis of the test results, simple design equations were proposed to predict the bond and end-bearing strength of GFRP spliced bars. There are, however, other parameters that need to be addressed related to the compression splice, such as confinement, bar diameter, concrete cover, concrete strength, and bar surface treatment. More experimental evidence and research are needed to accurately derive a design equation to predict the required splice length for GFRP bars under compression.

Acknowledgments

The authors wish to acknowledge the financial support of the Natural Sciences and Engineering Research Council of Canada (NSERC), the NSERC Research Chair in Innovative FRP Reinforcement for Concrete Structures, the Fonds de la recherche du Quebec en nature et technologies (FRQ-NT), and the Quebec Ministry of Transportation. The authors would like to thank Pultrall Inc. (Thetford Mines, QC, Canada) for donating the GFRP reinforcement and the technical staff of the structural & materials lab in the Department of Civil Engineering at the University of Sherbrooke.

References

ACI Committee 440. Guide for the Design and Construction of Structural Concrete Reinforced with FRP Bars (ACI 440.1R-15). Farmington Hills, MI: American Concrete Institute; 2015.

Zadeh HJ, Nanni A. Flexural stiffness and second-order effects in fiber-reinforced polymer-reinforced concrete frames. ACI Struct J 2017;114:533–44.

Razaqpur AG, Spadea S. Shear Strength of FRP Reinforced Concrete Members with Stirrups. J Compos Constr 2015;19.

Tottori S, Wakui H. Shear capacity of RC and PC beams using FRP reinforcement. ACI Sp 1993;138:615–31.

Guadagnini M, Pilakoutas K, Waldron P. Shear Resistance of FRP RC Beams: Experimental Study. J Compos Constr 2006;10:464–73.

Ali AH, Mohamed HM, Benmokrane B. Shear Behavior of Circular Concrete Members Reinforced with GFRP Bars and Spirals at Shear Span-to-Depth Ratios between 1.5 and 3.0. J Compos Constr 2016;18:1–10.

Bentz EC, Massam L, Collins MP. Shear Strength of Large Concrete Members with FRP Reinforcement. J Compos Constr 2010;14:637–46.

El-Gamal S, El-Salakawy E, Benmokrane B. Brhaviour of restrained concrete bridge deck slabs reinforced with FRP reinforcing bars under concentrated loads, El-Gamal.pdf. ACI Struct J 2005:727–35.

El-Sayed AK, El-Salakawy EF, Benmokrane B. Shear strength of fibre-reinforced polymer reinforced concrete deep beams without web reinforcement. Can J Civ Eng 2012;39:546–55.

Farghaly A, Benmokrane B. Shear Behavior of Large Reinforced Concrete Beams without Web Reinforcement. J Compos Constr 2013;17:1–10.

Hassan M, Ahmed E, Benmokrane B. Punching Shear Strength of Flat Slabs Reinforced with Glass Fibre-Reinforced Polymer (GFRP) Bars. Compos Constr 2014;19:1–10.

Luca A De, Matta F, Nanni A. Behavior of Full-Scale Glass Fiber-Reinforced Polymer Reinforced Concrete Columns under Axial Load. ACI Struct J 2010:589–96.

Tobbi H, Farghaly AS, Benmokrane B. Behavior of Concentrically Loaded Fiber-Reinforced Polymer Reinforced Concrete Columns with Varying Reinforcement Types and Ratios. ACI Struct J 2014;111:375–86.

Afifi MZ, Mohamed HM, Benmokrane B. Axial Capacity of Circular Concrete Columns Reinforced with GFRP Bars and Spirals. J Compos Constr 2014;18:1–11.

Afifi MZ, Mohamed HM, Chaallal O, Benmokrane B. Confinement Model for Concrete Columns Internally Confined with Carbon FRP Spirals and Hoops. J Struct Eng 2014;141:04014219.

Hadi MNS, Hasan HA, Sheikh MN. Experimental Investigations on Circular Concrete Columns Reinforced with GFRP Bars and Helices under Different Loading Conditions. J Compos Constr 2016;20:1–12.

Hadhood A, Mohamed HM, Benmokrane B. Failure Envelope of Circular Concrete Columns Reinforced with Glass Fiber-Reinforced Polymer Bars and Spirals. ACI Struct J 2017;114:1417–28.

Hadhood A, Mohamed HM, Benmokrane B. Experimental Study of Circular High-Strength Concrete Columns Reinforced with GFRP Bars and Spirals under Concentric and Eccentric Loading. J Compos Constr 2017;21.

Hadhood A, Mohamed HM, Benmokrane B. Axial Load–Moment Interaction Diagram of Circular Concrete Columns Reinforced with CFRP Bars and Spirals: Experimental and Theoretical Investigations. J Compos Constr 2017;21:1–12.

Pfister JP, Mattock AH. High Strength Bars as Concrete Reinforcement, Part 5:Lap splices in concentrically loaded columns. J PCA Res Dev Lab 1963;5:27–40.

ASTM. Standard Test Method for Tensile Properties of Fiber Reinforced Polymer Matrix. vol. i. West Conshohocken, PA: ASTM D7205M-06; 2011.

Chun S, Lee S, Oh B. Compression Lap Splice in Unconfined Concrete of 40 and 60 MPa (5800 and 8700 psi) Compressive Strengths. ACI Struct J 2010;107:170–8.

Beskos DE. Fracture of plain concrete under biaxial stresses. Cem Concr Res 1974;4:979–85.

Kupfer HB, Gerstle KH. Behavior of Concrete Under Biaxial Stresses. ACI J 1969;66:656–66.

Richart F, Brandtzaeg A, Brown RL. A Study of the Failure of Concrete under Combined Compressive Stresses. Univ Illinois Bull 1928;26:1–104.